Inorganic Chemistry

Article

pubs.acs.org/IC

Synthesis and Photobiological Activity of Ru(II) Dyads Derived from Pyrrole-2-carboxylate Thionoesters

Deborah A. Smithen,[†] Huimin Yin,[‡] Michael H. R. Beh,[†] Marc Hetu,[‡] T. Stanley Cameron,[†] Sherri A. McFarland,[*,‡,§] and Alison Thompson[*,†]

[†]Department of Chemistry, Dalhousie University, P.O. Box 15000, Halifax, Nova Scotia B3H 4R2, Canada

[‡]Department of Chemistry, Acadia University, 6 University Avenue, Wolfville, Nova Scotia B4P 2R6, Canada

[§]Department of Chemistry and Biochemistry, University of North Carolina at Greensboro, 301 McIver Street, Greensboro, North Carolina 27402, United States

Supporting Information

ABSTRACT: The synthesis and characterization of a series of heteroleptic ruthenium(II) dyads derived from pyrrole-2-carboxylate thionoesters are reported. Ligands bearing a conjugated thiocarbonyl group were found to be more reactive toward Ru(II) complexation compared to analogous all-oxygen pyrrole-2-carboxylate esters, and salient features of the resulting complexes were determined using X-ray crystallography, electronic absorption, and NMR spectroscopy. Selected complexes were evaluated for their potential in photobiological applications, whereupon all compounds demonstrated in vitro photodynamic therapy effects in HL-60 and SK-MEL-28 cells, with low nanomolar activities observed, and exhibited some of the largest photocytotoxicity indices to date (>2000). Importantly, the Ru(II) dyads could be activated by relatively soft doses of visible (100 J cm^{-2}, 29 mW cm^{-2}) or red light (100 J cm^{-2}, 34 mW cm^{-2}), which is compatible with therapeutic applications. Some compounds even demonstrated up to five-fold selectivity for malignant cells over noncancerous cells. These complexes were also shown to photocleave, and in some cases unwind, DNA in cell-free experiments. Thus, this new class of Ru(II) dyads has the capacity to interact with and damage biological macromolecules in the cell, making them attractive agents for photodynamic therapy.

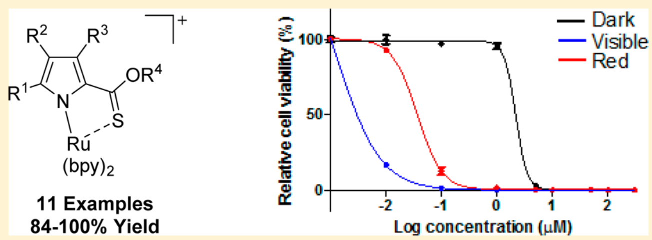

■ INTRODUCTION

The biological activity of transition-metal complexes (TMCs) has emerged as a major research focus in recent decades, particularly as metal-based scaffolds can offer significant advantages over organic compounds with regard to therapeutic and diagnostic applications.[1] Investigations concerning TMCs as anticancer agents are increasingly prominent,[2] with platinum- and ruthenium-based coordination complexes being the most widely studied.[3,4] In fact a large body of work exists regarding cytotoxic metal-based anticancer compounds, which is too exhaustive to cover here.[5−7] Certain Ru complexes, namely, NAMI-A, KP1019, and its sodium salt IT-139 (formerly called NKP-1339), have been investigated in clinical trials as single-agent, cytotoxic, or anti-metastatic alternatives to Pt-derived drugs.[8] Indeed, while NAMI-A and KP1019 fell short of expectations in Phase I studies, IT-139 exhibited a manageable safety profile alongside promising single-agent anticancer activity and is currently under development as a multimodal anticancer drug. Unlike their Pt counterparts, Ru complexes feature three-dimensional chiral cations that can be designed to exhibit desirable aqueous solubility. Their modular architectures enable facile chemical modifications through derivatization of one or more ligands to sample endless molecular and chemical space with electronic properties of biological relevance. In addition, the expanded octahedral coordination environment of Ru affords access to a larger number of geometric isomers and stereoisomers for increased site discrimination toward biological targets, as well as to multiple oxidation states for in vivo activation.[9,10]

Ru compounds have also been extensively investigated as light-responsive prodrugs for photodynamic therapy (PDT).[10−14] Briefly, PDT employs a nontoxic photosensitizer (PS) that is triggered by light to generate cytotoxic reactive oxygen species (ROS), notably singlet oxygen ($^1O_2$).[15,16] The advantage of PDT over traditional forms of cancer therapy (i.e., chemotherapy and radiotherapy), and more recently immunotherapy, is that it is highly selective, with toxicity confined to tissue where PS, light, and oxygen overlap spatiotemporally. In other words, off-site toxicity can be minimized by judicious control of the light delivery. Moreover, PDT is also known to invoke innate and adaptive antitumor immunity in addition to destruction of primary tumors and tumor vasculature.[17−20] Despite its potential, PDT is limited by the poor chemical characteristics of the few approved clinical PSs to date.[18,19] These PSs are organic structures that require molecular oxygen

Received: January 16, 2017
Published: March 16, 2017

DOI: 10.1021/acs.inorgchem.7b00072
Inorg. Chem. 2017, 56, 4121−4132

to exert a cytotoxic effect, thus precluding the treatment of hypoxic tissue, and cannot be activated by wavelengths of light that penetrate tissue best (700–900 nm).

Ru complexes have the potential to overcome these drawbacks. One such compound (TLD1433)[14] and its proprietary light device has entered a Phase 1/2a clinical trial for treating nonmuscle invasive bladder cancer with PDT (ClinicalTrials.gov Identifier: NCT03053635). This Ru-based compound belongs to a class of PSs called metal–organic *dyads*, which contain π-expansive organic chromophores tethered to neutral 2,2′-bipyridine (bpy), 1,10-phenanthroline (phen), or imidazo[4,5-*f*][1,10]phenanthroline (IP) ligands. These Ru dyads are characterized by low-lying triplet intraligand (^{3}IL) excited states with prolonged intrinsic lifetimes (tens to hundreds of microseconds) that are extremely sensitive to trace oxygen and other quenchers, yielding very potent PDT effects even at low oxygen tension, as well as oxygen-independent excited-state reactivity.[14,21−23] These and other Ru-based PSs investigated as PDT agents have mostly employed neutral diimines as auxiliary ligands with absorption maxima less than 500 nm but can be activated effectively with red light, most likely due to direct triplet–triplet absorption that populates these highly effective excited states.

There has been some interest in cyclometalated Ru complexes for PDT, because they exhibit bathochromic shifts in their longest wavelength absorption maxima by more than 100 nm relative to their diimine counterparts.[24−26] However, the lower-energy metal-to-ligand charge transfer (MLCT) transitions that are responsible for the longer wavelength absorption by cyclometalated Ru complexes also produce excited-state lifetimes that are much shorter due to the energy gap law, which limits the time available for bimolecular excited-state reactions that would be operative in PDT. In addition, some cyclometalated Ru systems were shown to be dark cytotoxic toward various cancer cell lines.[27] Presumably, these two factors are responsible for some of the very small in vitro PDT effects reported[24] and the perception that such systems are less useful for PDT. More recently, we demonstrated that some cyclometalated Ru C^N complexes derived from deprotonated phenylpyridine (phpy$^-$) and π-expansive organic chromophores yield in vitro PDT profiles that are as good as (or better than) some of our best Ru polypyridyl complexes.[21] This finding sparked an interest in cyclometalated systems involving the widely studied organometallic C^N motif and other anionic ligands such as the pyrrolide anion.

The organometallic chemistry of the pyrrolide anion, though formally isoelectronic with and geometrically comparable to the well-established cyclopentadienyl ligand,[28,29] is considerably underdeveloped.[30,31] This lack of interest may stem from historical reports that describe pyrrolide–metal complexes as intrinsically unstable and difficult to handle.[32,33] Since then, numerous pyrrolide-containing metal complexes have been reported: the ligands are often di- and cyclic tetrapyrroles as opposed to the simple pyrrolic system, in which the pyrrolide anion may adopt both σ- and π-bonding modes, thus enhancing the chemical reactivity of the metal and providing it with significant steric and electronic flexibility.[34,35] We recently reported the synthesis of the first heteroleptic pyrrolide 2,2′-bpy complexes of Ru(II).[36] These complexes, formed via chelation of the metal center to the pyrrolide N-atom as well as the oxygen atom of the carbonyl moiety of 2-formyl, 2-keto, and 2-carboxylato pyrroles, were found to be air- and moisture-stable, and were synthesized in excellent yields in all but the latter case, whereby attempts garnered success only in the case of electron-deficient pyrroles, specifically, those bearing halo-substituents about the pyrrole ring. This was thought to be the result of the electron-withdrawing ester moiety having a destabilizing effect on the Ru–O bond, a trend also observed in a study concerning rhenium complexes of pyrrolide ligands.[37] Cognizant that thiocarbonyl compounds typically display greater reactivity than their all-oxygen counterparts, likely due to the larger covalent radius and thus higher polarizability of the sulfur atom relative to oxygen, we hypothesized that conjugated pyrrolic thionoesters would act as improved ligands for Ru complexation. Herein, we report the synthesis and characterization of a family of these Ru(II) pyrrolic thionoester dyads and explore the potential of such complexes to act as PSs for PDT.

■ RESULTS AND DISCUSSION

Synthesis and Characterization. Initial efforts sought to confirm previous findings that 2-carboxylate pyrroles, in the absence of additional electron-withdrawing substituents, act as poor ligands for Ru complexation.[36] Using slightly modified conditions, we thus explored the reaction of a simple trialkyl-substituted pyrrolic ester (**1a**), obtained via Knorr-type condensation,[38] with $Ru(bpy)_2Cl_2$ under microwave irradiation. With the aim of providing stable, highly crystalline Ru(II) dyads that were soluble in organic solvents and thus facile to characterize, the bis(bpy) Ru(II) chloride salt **2a•Cl**, generated in situ, was converted to the hexafluorophosphate salt upon treatment with NH_4PF_6. The resulting bis(bpy) Ru(II) salt **2a•PF$_6$** was isolated, albeit in low yield, following purification via column chromatography (20%, Scheme 1). While low, this

Scheme 1. Synthesis of Ru(II) Complexes Derived from 2-Carboxylate (1a) and 2-Thiocarboxylate (3a) Pyrroles, Isolated as Their Hexafluorophosphate Salts

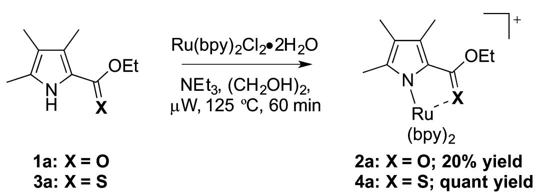

yield was a marked improvement on previous attempts[36] to complex alkyl 2-carboxylate pyrroles to Ru, an enhancement that was attributed to the modified isolation procedure that avoided trituration of the crude complex salt. It is also interesting to note that these low yields are in stark contrast to those obtained for trialkyl-substituted 2-formyl or keto pyrroles, which were shown to be highly effective ligands for Ru complexation.[36]

Complexation of the analogous thionoester (**3a**)[39] was subsequently examined. Vastly superior yields for chelation to Ru(II) emerged, as appreciated through comparison of complexation yields for **1a** and **3a**. Following the procedure described above, **4a•PF$_6$** was isolated in quantitative yield (Scheme 1). To the best of our knowledge, this is the first reported example of a metal complex featuring a pyrrolide ligand chelated through bidentate coordination involving the sulfur moiety of a pyrrole-2-carboxylate thionoester. In addition to the difference in isolated yields attained (Scheme 1), the pyrrolic ester- and thionoester-derived complexes (**2a** and **4a**) also differed in appearance with the former observed to be deep

DOI: 10.1021/acs.inorgchem.7b00072
Inorg. Chem. 2017, 56, 4121–4132

purple in the solid state and the latter deep red, with the variation more apparent in solution, whereupon the colors were more vibrant.

Subtle differences were also observed in the NMR spectra of these two dyads. Formation of heteroleptic $[Ru(bpy)_2(LL)]^{2+}$ complexes produces nonequivalence in all protons, leading to highly complex ^1H and ^{13}C NMR spectra, particularly in the aromatic regions. However, analysis of the alkyl-derived peaks in the ^1H NMR spectra revealed that replacing the carbonyl group of **2a** with a thiocarbonyl group (**4a**) resulted in a deshielding effect upon nearby *O*-CH_2CH_3 protons (Table 1, entries 4 and 5), yet did not significantly affect the environment of the pyrrolic methyl substituents (Table 1, entries 1−3), a trend also observed for the respective ligands (**1a** and **3a**).

Table 1. Comparison of NMR Chemical Shifts of Pyrrole Substituents in Complexes 2a and 4a, and Their Respective Ligands

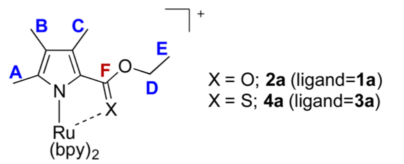

		NMR chemical shift (ppm)[a]			
		ligand[a]		Ru(II) complex[b]	
entry	group	**1a**[40]	**3a**	**2a**	**4a**
1[c]	**A** (CH_3)	2.18	2.19	1.14	1.19
2[c]	**B** (CH_3)	1.91	1.91	1.82	1.78
3[c]	**C** (CH_3)	2.25	2.25	2.19	2.24
4[c]	**D** (CH_2)	4.29	4.66	4.3−4.1	4.6−4.4
5[c]	**E** (CH_3)	1.34	1.46	1.17	1.42
6[d]	**F** (C═X)	161.9	199.5	172.8	194.7

[a]Solutions in $CDCl_3$. [b]Spectra recorded for PF_6 salts using CD_2Cl_2 as solvent. [c]Chemical shifts (^1H). [d]Chemical shifts (^{13}C).

Examination of the ^{13}C NMR spectra revealed a similar deshielding effect on the C = X group when moving from a carbonyl to a thiocarbonyl group (Table 1, entry 6). In the case of ligands **1a** and **3a**, the difference in chemical shift was as expected based on theoretical studies that suggest a linear relationship between $^{13}C{=}O$ and their corresponding $^{13}C{=}S$ values, conforming reasonably well to the equation $\delta(C{=}S) = 1.75\ \delta(C{=}O) - 79.7$.[41] Employing this equation provides a calculated value of 203.6 ppm for the C═S group of **3a**, comparable to the experimental value of 199.5 ppm. Conversely, in the case of Ru(II) complexes **2a** and **4a** the experimental value of 194.7 ppm for the C═S group of **4a** did not compare well with the calculated value of 222.7 ppm, suggesting that Ru complexation mitigates the deshielding effect.

X-ray Structure. An X-ray crystal structure was obtained for the complex **4a**, as the racemate, which confirmed the binding mode of the ligand and enabled structural analysis. Slow evaporation of a solution of **4a** in methanol generated dark red crystals that were suitable for analysis via X-ray diffraction. Solving the structure revealed that complex **4a** crystallizes in the monoclinic space group *C*2/*c*, with the Ru(II) center adopting a distorted octahedral geometry (Figure 1a).

The four Ru−N_{bpy} bonds are in the range of 2.048(3)−2.070(2) Å, well within normal limits compared to the parent Ru(II) tris(2,2′-bpy) complex[42] and similar heteroleptic Ru(II) bis(2,2′-bpy) dipyrrinato[43,44] or pyrrolide[36] complexes. The Ru−N_{pyr} bond length for **4a** is 2.091(2) Å, marginally longer than those found in similar ruthenium−pyrrole complexes bearing *α*-formyl (CHO) or ester (C(O)OR) groups in place of the thionoester (C(S)OR) moiety (Figures 1b, 5, and 6).[36] The Ru−N_{pyr} bonds of known pyrrolide and dipyrrinato derivatives are reported in the range of 2.076(2)−2.087(3) Å. The C^5−S bond of complex **4a** (1.700(3) Å) is similar in length to that of uncoordinated pyrrole **7** (1.650(2) Å),[45] but it is ∼0.4 Å longer than the carbonyl C^5−O bond of ester (**5**) and formyl (**6**) derivatives. The Ru−S bond of **4a** is also longer (2.365(1) Å) than the Ru−O bond of analogous 2-carboxylate pyrrole complex **5** (2.128(1) Å), which is again longer than that of the 2-formyl pyrrole−ruthenium complex **6** (2.097(2) Å). The bond length from C^1 to C^5 in compound **4a**, formally a C−C single bond, is 1.396(5) Å, making it slightly shorter than that of uncoordinated pyrrole **7** (1.432(2) Å), which would suggest an increase in double-bond character as would be typical for the azafulvenium resonance form of the pyrrolide ligand. The N_{pyr}−Ru−S bond angle is 82.64(8)°, which is larger than the N_{bpy}−Ru-N_{bipy} bond angles in complex **4a** (78.2(1)° and 79.0(1)°), akin to the bond angles in the ester and formyl derivatives (**5** and **6**). However, the Ru−S−C^5 bond angle (98.9(1)°) is smaller than the Ru−O−C^5 bond angle of the ester and formyl derivatives (**5** and **6**).

Following the success of initial efforts in confirming our hypothesis that pyrrole-2-thionoesters give higher yields for

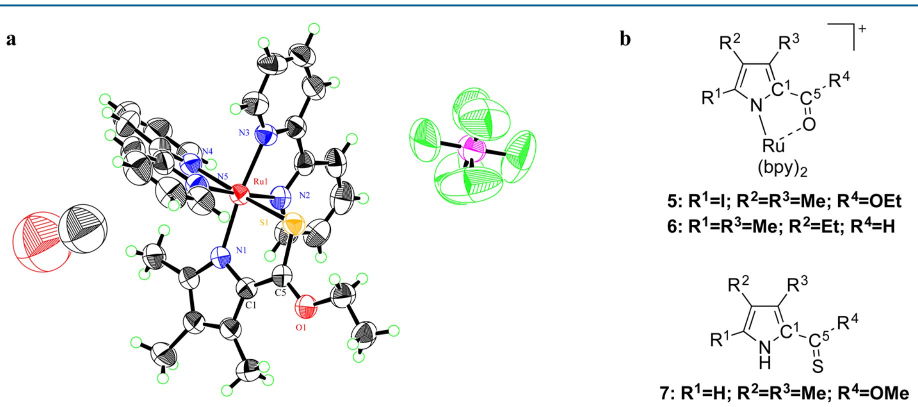

Figure 1. (a) X-ray structure of complex **4a** (50% probability ellipsoids) with PF_6^- counterion. (b) Related literature compounds with published solved crystal structures.

DOI: 10.1021/acs.inorgchem.7b00072
Inorg. Chem. 2017, 56, 4121−4132

Table 2. Synthesis of Pyrroles (3) and Corresponding Ru(II) Complexes (4)

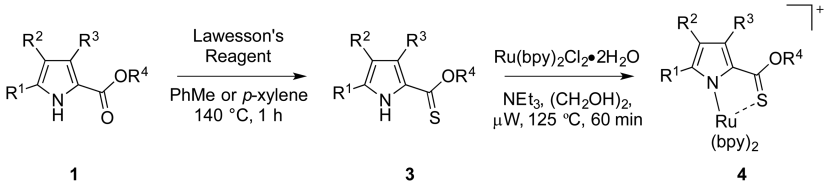

entry	pyrrole	R^1	R^2	R^3	R^4	yield **3** (%)[a]	yield **4** (%)[a,b]
1	**1a**	Me	Me	Me	Et	72 (**3a**)	quant (**4a**)
2	**1b**	Me	Me	Me	Bn	49 (**3b**)	quant (**4b**)
3	**1c**	Me	H	Me	Et	72 (**3c**)	quant (**4c**)
4	**1d**	Me	H	Me	Bn	50 (**3d**)	quant (**4d**)
5	**1e**	Me	Me	Et	Et	59 (**3e**)	quant (**4e**)
6	**1f**	Me	Me	Et	Bn	47 (**3f**)	93 (**4f**)
7	**1g**	H	Me	Me	Et	58 (**3g**)	quant (**4g**)
8	**1h**	Me	$(CH_2)_4CH_3$	Me	Et	64 (**3h**)	quant (**4h**)
9	**1i**	Me	$(CH_2)_2CH_3$	$(CH_2)_2CH_3$	Et	68 (**3i**)	quant (**4i**)
10	**1j**	Me	CO_2Et	Me	Et	52 (**3j**)[c]	quant (**4j**)
11	**1k**	Me	Ph	Me	Bn	55 (**3k**)[c]	84 (**4k**)

[a]Isolated yield. [b]Compounds isolated as their PF_6 salts. [c]Reaction time of 4 h.

complexation to Ru(II) compared to their all-oxygen analogues, we examined a series of pyrrolic thionoesters in the complexation reaction, to assess the substrate scope. Starting with the alkyl 2-carboxylate pyrroles (**1**), the corresponding thionocarbonyl pyrroles (**3**) were prepared in good yield after treatment with Lawesson's reagent at elevated temperature[39] (Table 2).

The thionoester-bearing pyrroles (**3**) were then examined as ligands in the microwave-assisted Ru(II) complexation reaction as per Scheme 1, providing the corresponding PF_6 salts in excellent yields (84%-quant, Table 2). This demonstrates that the complexation reaction is tolerant of a wide variety of structural features, including both ethyl and benzyl thionoesters (compare Table 2, entries 1 and 2; Table 2, entries 3 and 4; Table 2, entries 5 and 6), α- and β-free pyrroles (Table 2, entries 3, 4 and 7), long-chain alkyl substituents (Table 2, entries 8 and 9), electron-withdrawing substituents (Table 2, entry 10), and aryl substituents (Table 2, entry 11). In the case of the Ru(II) complex **4k** a notably lower yield was obtained (84%, Table 2, entry 11), which can presumably be ascribed to electronic effects, owing to the incorporation of a conjugated aryl substituent, which may contribute to a destabilizing effect on the Ru−S bond. All complexes synthesized (**4a**−**4k**) were fully characterized and moisture- and air-stable.

Electronic Absorption. As expected, the longest wavelength absorption maxima for these cyclometalated systems were shifted by up to 100 nm relative to typical Ru(II) complexes derived from neutral diimine-based ligands,[46] and their extinction coefficients were very similar to that of Photofrin[47] at wavelengths where clinical PDT is currently delivered (~630 nm). The absorption spectra of the Ru(II) complexes featuring pyrrolide ligands 2-substituted with ester (**2a**) and thionoester (**4a**−**k**) moieties revealed intense bands in the UV, characteristic of internal $\pi-\pi^*$ ligand-centered transitions, and lower-energy MLCT transitions in the visible region.

Electronic absorption spectra for the ester-coordinated complex **2a** and the analogous thionoester complexes (**4**) revealed significant differences in the absorption profiles (Figure 2). Most notably, thionoester-containing complex **4a** exhibits increased molar absorptivity, relative to the corresponding ester **2a**, in the high-energy MLCT transitions designated $Ru^{II}(d\pi) \rightarrow$ LL parentage (320−400 nm);[48] in the band centered around 430 nm attributed to the $n-\pi^*$ transition of the thiocarbonyl group[49] and, to a lesser extent, the lower-energy MLCT bands (≥575 nm) that can be assigned to overlapping $Ru(d\pi) \rightarrow bpy(\pi^*)$ (symmetric) and $Ru^{II}(d\pi) \rightarrow bpy(\pi^*)$ (antisymmetric) transitions.[48,50,51] However, the bathrochromic shift of ~25 nm in the longest wavelength $Ru(d\pi) \rightarrow bpy(\pi^*)$ absorption maximum for **2a** produced slightly larger extinction coefficients between 550 and 575 nm. Otherwise the local maxima were similar for the ester and thionoester congeners. Comparison of the absorption spectra obtained for Ru(II) complexes featuring ethyl (**4a**) and benzyl (**4b**) thionoester pyrrolide ligands showed no significant differences between the two. Comparing complexes with pyrrolides bearing β-alkyl (**4b**) and aryl (**4k**) substituents revealed similar profiles, although generally higher absorptivity was observed in the latter case (Figure 2).

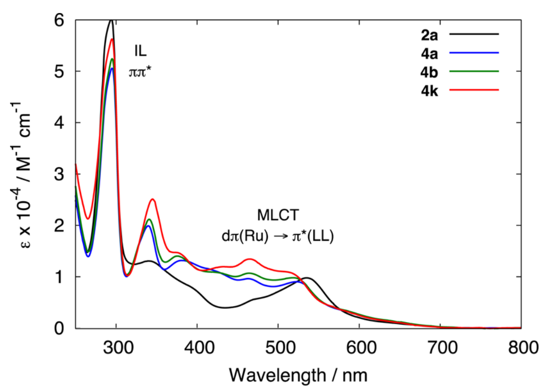

Figure 2. UV−vis spectra comparing the absorption profiles of ester (**2**) and thionoester (**4**) pyrrolide Ru(II)·PF_6 complexes in CH_2Cl_2, with labeled transitions.

Photobiology. Six of the Ru(II) complexes featuring 2-thionoester pyrrolide ligands were selected for photobiological studies (**4a**−**c**, **4h**, **4j**,**k**); these samples represent both ethyl and benzyl thionoesters, and bear distinct structural features

DOI: 10.1021/acs.inorgchem.7b00072
Inorg. Chem. 2017, 56, 4121−4132

Table 3. Photobiological Activity of Selected 2-Thionoester Pyrrolide Ru(II) Complexes in HL-60 Cells, with PS-to-Light Interval of 16 h

	EC_{50} (μM)			EC_{50} (μM)		
compound[a]	dark	visible[b]	PI[c]	red[b]	PI[c]	SF[d]
4a	1.08 ± 0.03	0.108 ± 0.004	10	0.357 ± 0.014	3	0.4
4b	1.17 ± 0.07	0.012 ± 0.001	98	0.145 ± 0.003	8	2.0
4c	1.23 ± 0.40	0.161 ± 0.011	8	0.355 ± 0.008	3	5.1
4h	1.74 ± 0.07	0.042 ± 0.002	41	0.102 ± 0.016	17	1.4
4j	1.43 ± 0.06	0.076 ± 0.018	19	0.213 ± 0.005	7	2.9
4k	1.42 ± 0.07	0.014 ± 0.001	101	0.052 ± 0.003	27	0.2
cisplatin[e]	5.9 ± 0.1					

[a]Compounds screened as their chloride salts. [b]Light 100 J cm^{-2}. [c]PI = phototherapeutic index. [d]SF = The ratio of dark EC_{50} values of CCD-1064Sk and HL-60 cells. [e]Cisplatin is not a PS, but it serves as a control.

Table 4. Photobiological Activity of Selected 2-Thionoester Pyrrolide Ru(II) Complexes in SK-MEL-28 Cells, with PS-to-Light Interval of 16 h

	EC_{50} (μM)			EC_{50} (μM)		
compound[a]	dark	visible[b]	PI[c]	red[b]	PI[c]	SF[e]
4a	0.280 ± 0.028	0.004 ± 0.001	70	0.070 ± 0.007	4	1.4
4b	2.19 ± 0.19	0.001 ± 0.0001	2185	0.036 ± 0.002	61	1.1
4c	2.01 ± 0.17	0.014 ± 0.0002	144	0.141 ± 0.015	14	3.1
4h	1.09 ± 0.03	0.011 ± 0.002	99	0.040 ± 0.002	27	2.2
4j	2.07 ± 0.12	0.004 ± 0.001	518	0.211 ± 0.027	10	2.0
4k	0.281 ± 0.036	0.010 ± 0.0002	28	0.038 ± 0.004	7	1.2
cisplatin[d]	2.8 ± 0.1					

[a]Compounds screened as their chloride salts. [b]Light 100 J cm^{-2}. [c]PI = phototherapeutic index. [d]Cisplatin is not a photosensitizer, but it serves as a control. [e]SF = The ratio of dark EC_{50} values of CCD-1064Sk and SK-MEL-28 cells.

including H, alkyl, ester, and aryl substituents. The hexafluorophosphate salts of these complexes were converted to their biologically compatible, water-soluble chloride salts via treatment with excess tetrabutylammonium chloride, followed by purification using column chromatography (90%-quant yield, characterization details in Supporting Information). Successful counterion exchange was confirmed using electrospray ionization mass spectrometry (ESI-MS) in negative ion mode, which showed a disappearance of the signal corresponding to the PF_6^- anion. Four compounds have Me at both R^1 and R^3, and Et at R^4, and differ only at R^2: H (**4c**), Me (**4a**), $-(CH_2)_4CH_3$ (**4h**), or $-CO_2Et$ (**4j**). Two are identical at R^1 and R^3 (Me) and differ only at R^4: Et (**4a**) or Bn (**4b**). Another two are also identical at R^1 and R^3 (Me) and at R^4 (Bn), differing only at R^2: Me (**4b**) or Ph (**4k**). This small subset of compounds was chosen to determine the structure−activity effects with systematic changes to R^2 and R^4 and to highlight the utility of this new class of cyclometalated Ru(II) dyads for in vitro PDT (and, in some cases, as traditional but selective anticancer compounds).

The cytotoxicity and photocytotoxicity of these representative 2-thionoester pyrrolide Ru(II) dyads was assessed in three human cell lines (HL-60 promyelocytic leukemia cells, SK-MEL-28 melanoma cells, and CCD−1064Sk skin fibroblasts) according to an established in-house cellular assay.[9,52] Briefly, cells were dosed with metal complex (1 nM-300 μM) and incubated for 16 h at 37 °C prior to a light or sham (dark) treatment. The light treatment was 100 J cm^{-2} delivered from a broadband visible lamp (34 mW cm^{-2}) or red light-emitting diodes (LEDs) at 625 nm (29 mW cm^{-2}) over the course of 49 and 57 min, respectively. The complexes, as monitored by UV−vis absorption spectroscopy, exhibited no photobleaching upon exposure to 100 J cm^{-2} of visible or red light delivered at an irradiance of 34 and 29 mW cm^{-2}, respectively. Alamar Blue was added at 48 h post treatment, and cell viability was quantified 16 h later. Cells that were dosed at high concentrations of PS, where the PS interferes with absorption and emission of light by the cell viability dye, were also observed manually under a microscope. The effectiveness of the Ru(II) complexes as in vitro PDT agents was assessed by quantifying the dark and light cytotoxicity profiles as EC_{50} values (concentration required to reduce cell viability to 50%). Their photocytotoxicity indices (PIs) were then calculated as the ratio of dark to light EC_{50} values, reflecting the PDT therapeutic margin in a given cancer cell line. Dark EC_{50} values were also assessed using noncancerous skin fibroblasts (CCD−1064Sk) to determine any selective dark cytotoxicity toward cancer cells over normal cells. The selectivity factor (SF) is defined as the dark EC_{50} determined for CCD−1064Sk skin fibroblasts divided by the dark EC_{50} determined for a given cancer cell line. For comparison, larger PIs signify larger PDT effects, and SF values > 1 represent selectivity toward cancer cells. Note that, as long as the therapeutic dose is significantly less than the dark EC_{50} value of the normal cell line, it is not necessary to have inherent selectivity for cancer cells over normal cells. Rather, selectivity is achieved by spatial control of the light delivery.

As observed for some of the other classes of cyclometalated Ru(II) complexes, the in vitro cytotoxicity for the Ru(II) dyads derived from 2-thionoester pyrrolide ligands was high, with EC_{50} values as low as 280 nM in the absence of a light trigger. This cytotoxicity proved to be very sensitive to the substitution pattern about the pyrrole ring, and to the type of thionoester, in two of the three cell lines investigated. Dark EC_{50} values for HL-60, SK-MEL-28, and CCD−1064Sk cells ranged from 1.1−1.7, 0.28−2.2, and 0.35−6.3 μM, respectively (Tables 3, 4, and

DOI: 10.1021/acs.inorgchem.7b00072
Inorg. Chem. 2017, 56, 4121−4132

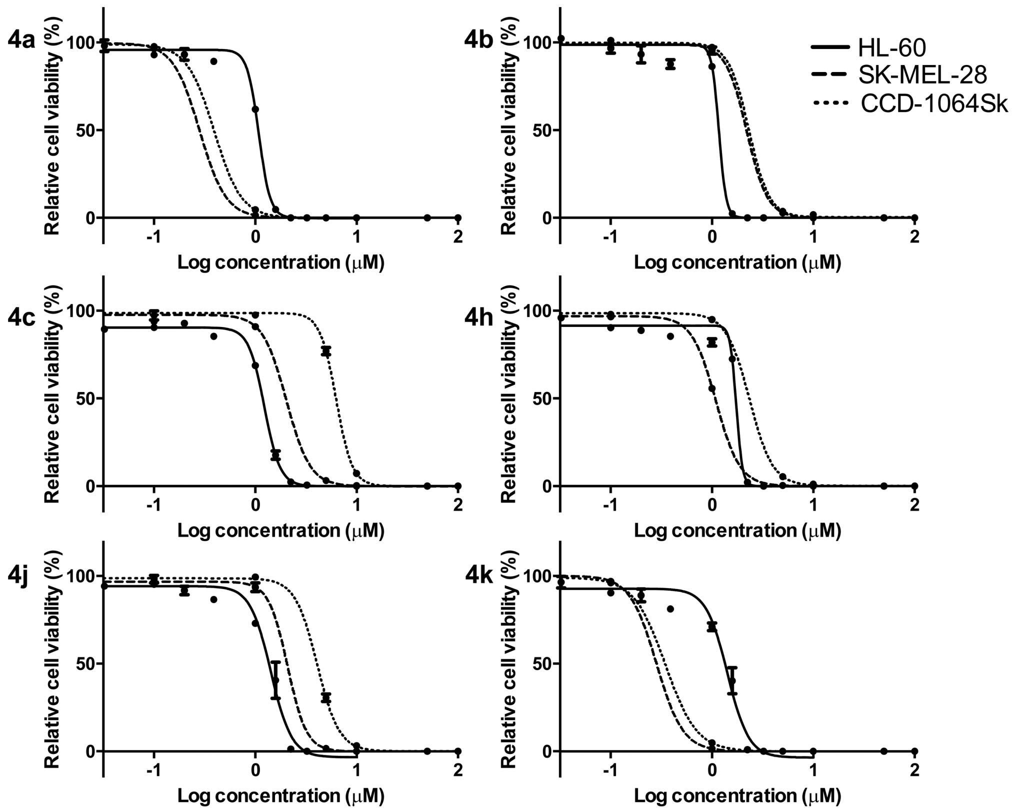

Figure 3. In vitro cytotoxicity curves for compounds **4a**−**c**, **4h**, **4j**, and **4k** in HL-60, SK-MEL-28, and CCD-1064Sk cells.

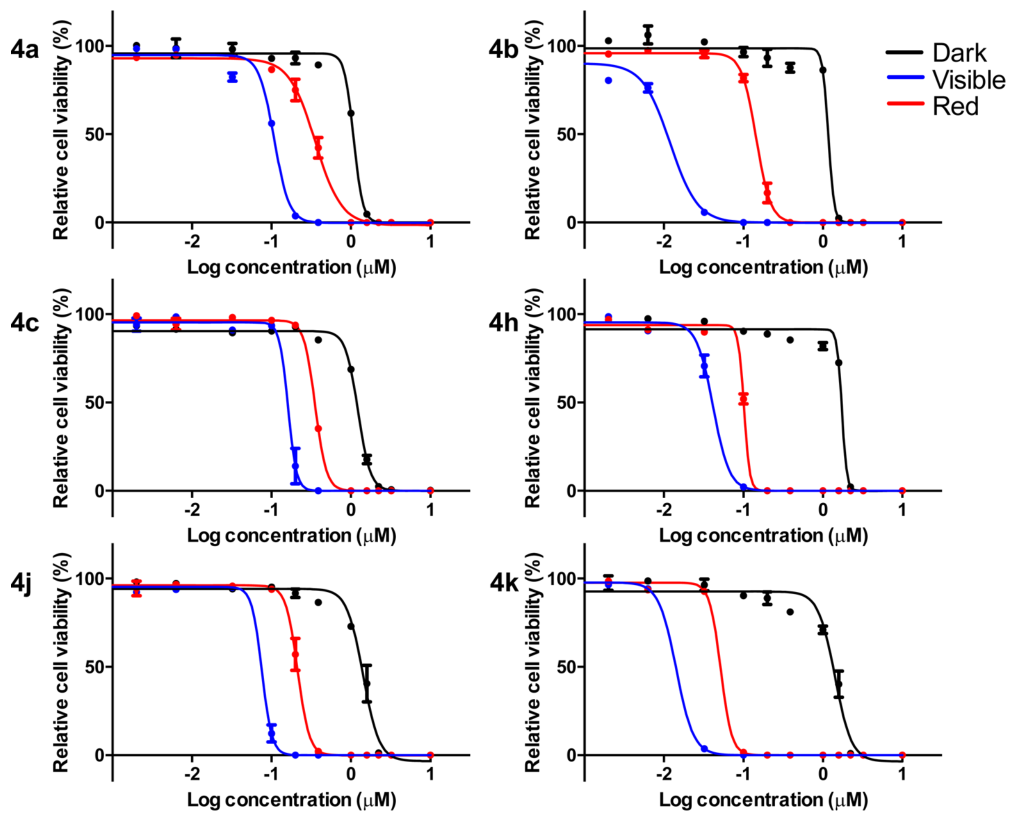

Figure 4. In vitro PDT dose−response curves for compounds **4a**−**c**, **4h**, **4j**, and **4k** in HL-60 cells, with visible (blue), red (red), or no (black) light activation.

S1). In SK-MEL-28 and CCD−1064Sk cells, where there was a much larger range of activities, **4a** and **4k** were the most cytotoxic, and **4c** and **4j** were the least cytotoxic (by 18-fold in CCD−1064Sk cells and 8-fold in SK-MEL-28 cells). Given that

DOI: 10.1021/acs.inorgchem.7b00072
Inorg. Chem. 2017, 56, 4121−4132

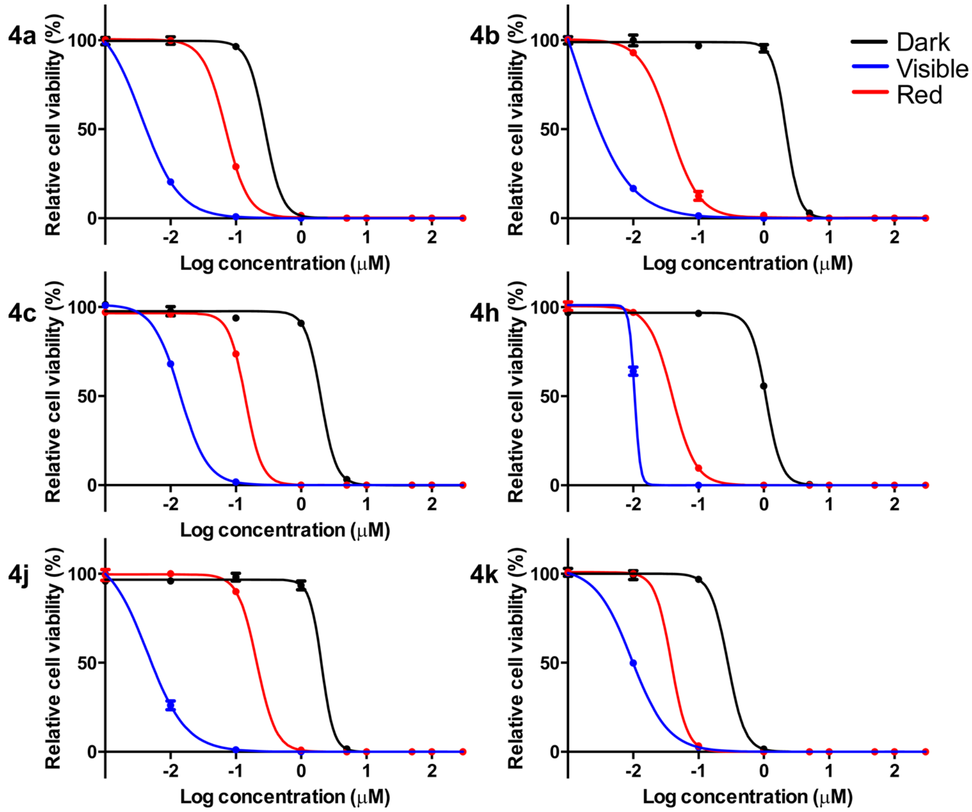

Figure 5. In vitro PDT dose−response curves for compounds **4a**−**c**, **4h**, **4j**, and **4k** in SK-MEL-28 cells, with visible (blue), red (red), or no (black) light activation.

4a (R^2 = Me) was one of the most cytotoxic compounds and **4c** (R^2 = H) and **4j** (R^2 = $-CO_2Et$) were the least dark toxic, the cytotoxicity is very sensitive to changes at R^2 when R^4 is Et. This is also the case when R^4 = Bn, supported by large differences between the cytotoxicities of **4b** and **4k**, with **4k** being more toxic by almost eight-fold. For the ethyl thionoesters, R^2 = Me produced potent dark toxicity (EC_{50} = 280 nM), while R^2 = H, $-(CH_2)_4CH_3$, or $-CO_2Et$ were less cytotoxic by ~10-fold. However, the presence of R^2 = Me in the benzyl thionoesters (EC_{50} = 2.2 μM) did not lead to nanomolar toxicity, yet R^2 = Ph did. The conclusion is that the nature of the substituent at R^4 influences the cytotoxic effects due to variances at R^2, and vice versa.

Notably, **4c** was up to 5 times more cytotoxic toward cancer cells relative to normal cells (SF = 5.1, HL-60), and **4j** was also selectively cytotoxic toward cancer cells but to a lesser extent (Figure 3). These ethyl thionoester complexes bearing R^2 = H or R^2 = $-CO_2Et$ were also the least cytotoxic in general. This selectivity, in addition to the observation that all of the compounds exhibit anticancer effects that surpass the gold standard cisplatin in both cancer cell lines studied (Tables 3 and 4), highlights the potential utility of these Ru(II) 2-thionoester pyrrolide dyads as traditional chemotherapeutics.

While the six complexes investigated acted as promising anticancer agents in the absence of a light trigger, this cytotoxicity was enhanced further with photoactivation using broadband visible or red light (Figures 4 and 5). The more energetic visible light produced smaller EC_{50} values for all of the complexes across all of the cell lines studied, but even red light produced PIs as large as 27 (**4k**) in HL-60 cells and greater than 60 (**4b**) in SK-MEL-28 cells (Tables 3 and 4). Both of these PI values are larger than that known for Photofrin (PI ≈ 10), albeit reported in a different cell line.[53] The relative ordering of the light EC_{50} values measured for the different compounds varied between the two cancer cell lines studied and between the two light conditions used, underscoring the importance of being cautious with generalizations regarding PS activity and structure−activity relationships. Nevertheless, some trends could be discerned.

With visible light activation, **4b** was exceptionally potent toward both cancer cell lines, with light EC_{50} values of 12 nM in HL-60 and 1 nM in SK-MEL-28, giving rise to PIs of 100 and greater than 2100, respectively (Tables 3 and 4). These large phototherapeutic margins afford the opportunity to deliver the PS at very low concentration, where it is completely nontoxic without the light trigger. One of the least active PSs in both cell lines with visible light activation was **4c** (EC_{50} = 161 nM, PI 8 in HL-60; EC_{50} = 14 nM, PI = 144 in SK-MEL-28), demonstrating that the least phototoxic PS in this series is still up to 300-fold more phototoxic than Photofrin. The trends for light potencies were as follows: **4b** ≈ **4k** > **4h** > **4j** > **4a** > **4c** (HL-60/visible PDT); **4k** > **4h** > **4b** > **4j** > **4c** ≈ **4a** (HL-60/red PDT); **4b** > **4a** = **4j** > **4k** ≈ **4h** > **4c** (SK-MEL-28/visible PDT); and **4b** ≈ **4k** ≈ **4h** > **4a** > **4c** > **4j** (SK-MEL-28/red PDT). The trends for the PI values were: **4k** ≈ **4b** > **4h** > **4j** > **4a** > **4c** (HL-60/visible PDT); **4k** > **4h** > **4b** ≈ **4j** > **4a** = **4c** (HL-60/red PDT); **4b** > **4j** > **4c** > **4h** > **4a** > **4k** (SK-MEL-28/visible PDT); and **4b** > **4h** > **4c** > **4j** > **4k** > **4a** (SK-MEL-28/red PDT).

The benzyl thionoesters (**4b** and **4k**) yielded the most potent visible light EC_{50} values and largest PIs in HL-60 cells. While benzyl thionoester **4b** also gave the most potent visible light EC_{50} values and largest PI in SK-MEL-28 cells, ethyl thionoester **4j** was also very potent. However, with red light

DOI: 10.1021/acs.inorgchem.7b00072
Inorg. Chem. 2017, 56, 4121−4132

activation in HL60 cells, ethyl thionoester **4h** surpassed **4b**. Close scrutiny revealed that the light-triggered activities of these Ru(II) dyads were sensitive to the cell line employed and the light treatment delivered. Nevertheless, **4b**, **4j**, and **4h** emerged as good in vitro PDT agents with low nanomolar potencies and highlight the potential utility of both ethyl and benzyl thionoester Ru(II) dyads for PDT applications given the ability to fine-tune the photocytotoxicity via substituent changes about the pyrrole ring. Current efforts are underway to understand the photophysical and photochemical differences that may give rise to these differences in photobiological activity, and to explore additional variations at R^2 and R^4.

A possible source of the observed in vitro PDT effects is the generation of reactive intermediates such as cytotoxic $^1O_2$, which can damage biological tissue and invoke cell death. Plasmid DNA serves as a convenient probe for testing the ability of PSs to photodamage biological macromolecules (regardless of whether DNA is the actual intracellular target). We used a DNA gel electrophoretic mobility shift assay[54−56] to study the six compounds that were evaluated for their in vitro PDT effects. The migration distance of pUC19 DNA through the agarose gel depends on its size and topological form, and this topology is acutely dependent on DNA interactions with exogenous agents. Undamaged DNA (supercoiled, Form I) migrates the farthest, while condensed/aggregated may not move from the loading well at all (Form IV). Single-strand breaks in the DNA backbone cause relaxation of the supercoils to produce an open circular form (Form II), which migrates between Form I and IV. Single-strand breaks that occur on opposite strands within ∼16 base pairs or frank double strand breaks yield linear DNA that migrates slightly more than Form II. The relative migration speed/distance follows: Form I > III > II > IV.

Briefly, pUC19 plasmid DNA (20 μM nucleotide phosphates) was exposed to increasing concentrations of the PS between 5 and 60 μM and then treated with visible light (14 J cm^{-2}) and electrophoresed on an agarose gel slab before or after staining with ethidium bromide (EB) for visualization of the DNA bands (Figure 6, lanes 3−10). The light-treated DNA samples were compared to untreated DNA (Figure 6, lane 1), DNA treated with light only (Figure 6, lane 2), or DNA exposed to PS at the highest concentration without the light treatment (Figure 6, lane 11). EB was added to the samples before (Figure 6, EB) or after (non-EB) electrophoresis to emphasize strand breaks and unwinding, respectively. All of the Ru(II) thionoester dyads produced single-strand breaks in DNA in a concentration-dependent manner upon light exposure (Figure 6, conversion of Form I to Form II), indicating that the compounds could potentially generate intracellular cytotoxic reactive intermediates. No Form III DNA could be discerned, but some of the compounds (**4b**, **4h**, **4k**) did cause condensation[57−59] (or aggregation) of the DNA (Form IV), while others (**4a**, **4c**, or **4j**) caused incomplete conversion to Forms II or IV. Compound **4b** caused complete conversion to Form II before condensation, while **4k** (and to a lesser extent **4h**) caused both to occur simultaneously. Three of the compounds (**4b**, **4c**, and **4h**) caused unwinding of the DNA helix (Figure 6, non-EB), but this interaction did not correlate with the potency of the compound in terms of DNA photodamage. The compounds that produced the most DNA damage (**4b**, **4h**, and **4k**) were also characterized by DNA band disappearance at the highest concentrations of PS employed with or without a light treatment. Such effects could stem from

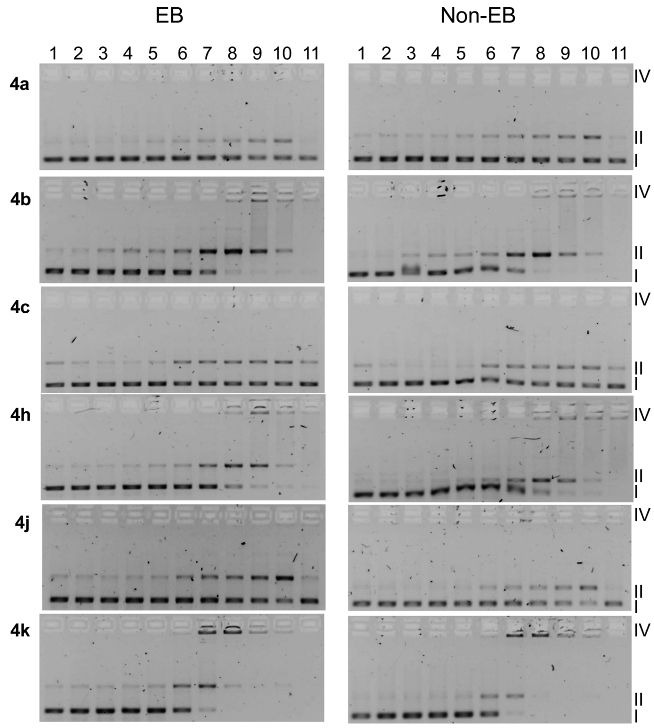

Figure 6. DNA photocleavage of pUC19 DNA (20 μM bases) dosed with metal complex (MC) **4a−c**, **4h**, **4j**, and **4k** with visible light (14 J cm^{-2}). Gel mobility shift assays employed 1% agarose gels (0.75 μgmL^{-1} EB) electrophoresed in 1X TAE at 8 V cm^{-1} for 30 min or gels were then stained in 5 μg mL^{-1} EB solution in water for 45 min, then destained in distilled water for 30 min. Lane 1, DNA only (−*hν*); lane 2, DNA only (+*hν*); lane 3, 5 μM MC (+*hν*); lane 4, 10 μM MC (+*hν*); lane 5, 15 μM MC (+*hν*); lane 6, 20 μM MC (+*hν*); lane 7, 30 μM MC (+*hν*); lane 8, 40 μM MC (+*hν*); lane 9, 50 μM MC (+*hν*); lane 10, 60 μM MC (+*hν*); lane 11, 60 μM MC (−*hν*). Forms I, II, and IV DNA refer to supercoiled plasmid, nicked circular plasmid, and aggregated plasmid, respectively.

fluorescence quenching of EB by distortion of the DNA helix and/or displacement of intercalated EB by the PS. The non-EB gels demonstrate the ability of some of the compounds to interact with DNA strongly enough to unwind it.

It is interesting to note that the estimated photoreactivities from the DNA gel mobility shift assays paralleled the in vitro light EC_{50} trends in HL-60 cells but not in SK-MEL-28 cells. The cell-free DNA damage experiment may not correlate with cellular PDT effects given that DNA might not be the intracellular biological target and that uptake, efflux, and metabolism affect such relationships. Regardless, the experiments point toward notable DNA interactions for this new class of compounds that includes light-induced single-strand breaks and condensation, as well as the ability to unwind the DNA helix. Whether some of these interactions (such as those observed in the dark for **4b**, **4h**, and **4k**) result in the observed dark cytotoxicity, relative to many of the non-cyclometalated Ru(II) systems, remains to be discovered.

■ CONCLUSION

A novel series of heteroleptic ruthenium(II) complexes derived from pyrrole-2-carboxylate thionoesters were synthesized in excellent yield, demonstrating that use of a thiocarbonyl group as a chelating moiety in the bidentate ligand system serves to address the problems of poor reactivity encountered with the

DOI: 10.1021/acs.inorgchem.7b00072
Inorg. Chem. 2017, 56, 4121−4132

analogous all-oxygen 2-carboxylate pyrroles. All complexes synthesized were characterized using ^{1}H and ^{13}C NMR and UV/vis spectroscopy, and X-ray crystallography was used to confirm the binding mode and gain structural information. Photobiological activity of selected complexes was assessed in HL-60 and SK-MEL-28 cells, and dark toxicity was further probed in normal skin fibroblasts. All of the compounds demonstrated in vitro PDT effects, and some were among the most potent reported to date. The selectivity exhibited by some of these novel Ru(II) dyads toward cancer cells, alongside their nanomolar activities, may prove useful in the search for chemotherapeutics with a considerably different mechanism of action than cisplatin in an effort to overcome the acquired or innate resistance to platinum-based cancer therapy. The low nanomolar photo-cytotoxicities and the very large photo-therapeutic margins could potentially offset the dark toxicity of the complexes, making them both excellent traditional anticancer compounds and PDT agents. The compounds also interacted strongly with DNA in cell-free experiments, indicating that DNA could be an intracellular target, but more importantly that all of the compounds are capable of generating potentially cytotoxic reactive intermediates for PDT. Dark and light EC_{50} values and PIs measured for the different compounds varied by cell line and by light treatment condition. The absence of systematic trends across all conditions precluded a generalized structure−activity assessment but highlights the rich diversity yet to be exploited in medicinal inorganic chemistry, as we hereby introduce a new class of cyclometalated Ru(II) dyads as PSs for in vitro PDT and possibly other applications. Efforts are underway to explore the cellular uptake profiles with and without a light trigger, the photophysical properties underlying the observed PDT effects, the PDT mechanism(s), and structure−activity relationships for this interesting compound class.

■ EXPERIMENTAL PROCEDURES

Full synthesis and characterization data can be found in the Supporting Information.

Bis(2,2′-bipyridyl)-(O-ethyl-3,4,5-trimethyl-2-carbothiolato-N-pyrrolato)ruthenium(II) (4a). Ru(II) complex **4a** was synthesized from ligand **3a** using general procedure 2 (see Supporting Information) and purified over silica, eluting with 0−4% *iso*-propyl alcohol (IPA)/CH_2Cl_2 to give complex salt **4a·PF$_6$** as a deep red crystalline solid (116 mg, 100% yield). mp 172−176 °C; ^{1}H NMR (CD_2Cl_2, 500 MHz) δ 9.34 (d, 1H, J = 5.5 Hz, ArH). 8.29 (at, 3H, J = 8.0 Hz, ArH), 8.18 (d, 1H, J = 8.0 Hz, ArH), 7.95−7.91 (m, 3H, ArH), 7.85 (t, 1H, J = 7.8 Hz, ArH), 7.77 (t, 1H, J = 7.8 Hz, ArH), 7.65 (d, 1H, J = 5.5 Hz, ArH), 7.53−7.49 (m, 2H, ArH), 7.43 (t, 1H, J = 6.5 Hz, ArH), 7.22 (t, 1H, J = 6.5 Hz, ArH), 7.11 (t, 1H, J = 6.5 Hz, ArH), 4.64−4.58 (m, 1H, CH_2CH$_3$), 4.49−4.43 (m, 1H, CH_2CH$_3$), 2.24 (s, 3H, CH_3), 1.78 (s, 3H, CH_3), 1.42 (t, 3H, J = 7.0 Hz, CH$_2$$CH_3$), 1.19 (s, 3H, CH_3) ppm, ^{13}C NMR (CD_2Cl_2, 125 MHz, udeft) δ 194.7, 158.3, 158.1, 158.0, 157.8, 155.6, 155.0, 152.7, 151.6, 150.9, 139.8, 136.3, 136.1, 135.5, 135.3, 131.4, 127.13, 127.06, 126.8, 126.7, 124.4, 123.6, 123.4, 123.24, 123.18, 67.4, 14.8, 13.4, 11.8, 9.6 ppm; ESI-MS$^+$: 610.1 (M)$^+$; high-resolution mass spectrometry (HRMS): 610.1206 Found, 610.1209 Calculated for $C_{30}H_{30}N_5SORu$; ESI-MS$^-$: 145.0 (PF_6)$^-$; $\varepsilon_{523\text{ nm}}$ 9100, $\varepsilon_{381\text{ nm}}$ 13 200, $\varepsilon_{340\text{ nm}}$ 19 900, $\varepsilon_{295\text{ nm}}$ 50 600 (CH_2Cl_2). The corresponding chloride salt (**4a·Cl**) was obtained using GP3 as a black solid (30 mg, 100%). mp/dp > 200 °C; ESI-MS$^+$: 610.1 (M)$^+$; ESI-MS$^-$: PF_6^- ion not observed. Crystal data for compound **4a·PF$_6$**: $C_{30.50}H_{32}F_6N_5O_{1.50}PRuS$, MM = 770.72 g/mol. Dark red pinacoid crystal, dimensions 0.35 × 0.27 × 0.18 mm; monoclinic space group, $C2/c$; a = 21.9599(9) Å, b = 13.8939(4) Å, c = 24.2344(10) Å, α = 90°, β = 115.9710(15)°, γ = 90°, V = 6647.4(4) Å^3, Z = 8, d = 1.540 g/cm^3, μ(Mo Kα) = 6.510 cm^{-1}, 19 764 reflections (7910 unique, R_{int} = 0.053), R = 0.0605, $wR2$ = 0.1642, goodness-of-fit = 1.043, R-factor = 5.17%. CCDC deposition number: 1485965.

Metal Compound Solutions. Stock solutions of the chloride salts of the Ru(II) complexes (**4·Cl**) were prepared at 5 mM in 10% dimethyl sulfoxide (DMSO) in water and kept at −20 °C prior to use. Working dilutions were prepared through dilution of the aqueous stock with pH 7.4 Dulbecco's phosphate buffered saline (DPBS). DPBS is a balanced salt solution of 1.47 mM potassium phosphate monobasic, 8.10 mM sodium phosphate dibasic, 2.68 mM potassium chloride, and 0.137 M sodium chloride (no Ca^{2+} or Mg^{2+}). DMSO in the assay wells was under 0.1% at the highest complex concentration.

HL-60 Cell Culture. HL-60 human promyelocytic leukemia cells (ATCC CCL-240) were cultured at 37 °C under 5% CO_2 in RPMI 1640 (Mediatech Media MT-10−040-CV) supplemented with 20% fetal bovine serum (FBS; PAA Laboratories, A15−701) and were passaged three to four times per week according to standard aseptic procedures. Cultures were started at 200 000 cells per milliliter in 25 cm^2 tissue culture flasks and were subcultured when growth reached 800 000 cells mL^{-1} to avoid senescence associated with prolonged high cell density. Complete growth medium was prepared in 200 mL portions as needed by combining RPMI 1640 (160 mL) and FBS (40 mL, prealiquoted, and heat inactivated) in a 250 mL Millipore vacuum stericup (0.22 μm) and filtering.

SK-MEL-28 Cell Culture. Adherent SK-MEL-28 malignant melanoma cells (ATCC HTB-72) were cultured in Eagle's Minimum Essential Medium (EMEM; Mediatech Media MT-10−009-CV) supplemented with 10% FBS and were incubated at 37 °C under 5% CO_2 and passaged two to three times per week according to standard aseptic procedures. SK-MEL-28 cells were started at 200 000 cells per milliliter in 75 cm^2 tissue culture flasks and were subcultured when growth reached 550 000 cells per milliliter by removing old culture medium and rinsing the cell layer once with Dulbecco's phosphate-buffered saline (DPBS 1X, Mediatech, 21−031-CV) followed by dissociation of cell monolayer with 1X Trypsin−EDTA solution (0.25% (w/v Trypsin/0.53 mM EDTA, ATCC 30−2101)). Complete growth medium was added to the cell suspension to allow appropriate aliquots of cells to be transferred to new cell vessels. Complete growth medium was prepared in 150 mL portions as needed by combining EMEM (135 mL) and FBS (15 mL, prealiquoted, and heat inactivated) in a 250 mL Millipore vacuum stericup (0.22 μm) and filtering.

CCD-1064Sk Cell Culture. Adherent CCD-1064Sk normal skin fibroblasts (ATCC CRL-2076) were cultured in Iscove's Modified Dulbecco's Medium (IMDM) supplemented with 10% FBS (PAA Laboratories, A15−701), incubated at 37 °C under 5% CO_2, and were passaged two to three times per week according to standard aseptic procedures. CCD-1064Sk cells were started at 200 000 cells per milliliter in 75 cm^2 tissue culture flasks and were subcultured when growth reached 550 000 cells per milliliter by removing old culture medium and rinsing the cell monolayer once with Dulbecco's phosphate-buffered saline (DPBS 1X, Mediatech, 21−031-CV), followed by dissociation of the cell monolayer with trypsin−ethylenediaminetetraacetic acid (EDTA) solution (0.25% w/v Trypsin/0.53 mM EDTA, ATCC 30−2101). Complete growth medium was added to the cell suspension to allow appropriate aliquots of cells to be transferred to new cell vessels. Complete growth medium was prepared in 150 mL portions as needed by combining IMDM (125 mL) and FBS (25 mL, prealiquoted, and heat inactivated) in a 250 mL Millipore vacuum stericup (0.22 μm) and filtering.

Cytotoxicity and Photocytotoxicity. Cell viability experiments were performed in triplicate in 96-well ultralow attachment flat bottom microtiter plates (Corning Costar, Acton, MA), where outer wells along the periphery contained 200 μL of DPBS (2.68 mM potassium chloride, 1.47 mM potassium phosphate monobasic, 0.137 M sodium chloride, and 8.10 mM sodium phosphate dibasic) to minimize evaporation from sample wells. Cells growing in log phase (HL-60 cells: ∼800 000 cells per milliliter, SK-MEL-28 and CCD-1064Sk cells: ∼550 000−600 000 cells per milliliter) with at least 93% viability were transferred in 50 μL aliquots to inner wells containing warm culture

DOI: 10.1021/acs.inorgchem.7b00072
Inorg. Chem. 2017, 56, 4121−4132

medium (25 μL) and placed in a 37 °C, 5% CO_2 water-jacketed incubator (Thermo Electron Corp., FormaSeries II, model 3110, HEPA Class 100) for 3 h to equilibrate (and allow for efficient cell attachment in the case of adherent cells). Ru-based compounds were serially diluted with DPBS and prewarmed at 37 °C before 25 μL aliquots of the appropriate dilutions were added to cells. PS-treated microplates were incubated at 37 °C under 5% CO_2 for 16 h drug-to-light intervals. Control microplates not receiving a light treatment were kept in the dark in an incubator, and light-treated microplates were irradiated under one of the following conditions: visible light (400−700 nm, 34.2 mW cm^{-2}) using a 190 W BenQ MS 510 overhead projector or red light (625 nm, 29.1 mW cm^{-2}) from an LED array (PhotoDynamic Inc., Halifax, NS). Irradiation times using these two light sources were ~49 and 57 min, respectively, to yield total light doses of 100 J cm^{-2}. Both untreated and light-treated microplates were incubated for another 48 h before 10 μL aliquots of prewarmed Alamar Blue reagent (Life Technologies DAL 1025) were added to all sample wells and subsequently incubated for another 15−16 h. Cell viability was determined on the basis of the ability of the Alamar Blue redox indicator to be metabolically converted to a fluorescent dye by only live cells. Fluorescence was quantified with a Cytofluor 4000 fluorescence microplate reader with the excitation filter set at 530 ± 25 nm and emission filter set at 620 ± 40 nm. EC_{50} values for cytotoxicity (dark) and photo-cytotoxicity (light) were calculated from sigmoidal fits of the dose−response curves using Graph Pad Prism 6.0 according to eq 1 (below), where y_i and y_f are the initial and final fluorescence signal intensities. For cells growing in log phase and of the same passage number, EC_{50} values are generally reproducible to within ±25% in the sub-micromolar regime, ±10% below 10 μM, and ±5% above 10 μM. Phototherapeutic indices (PIs), a measure of the therapeutic window, were calculated from the ratio of dark to light EC_{50} values obtained from the dose−response curves.

$$y = y_i + \frac{y_i - y_f}{1 + 10\exp[(\log EC_{50} - x) \times (\text{Hill slope})]} \quad (1)$$

DNA Mobility-Shift Assays. DNA modification by compounds **4a**−**c**, **4h**, **4j**, and **4k** was assessed according to a general plasmid DNA gel mobility shift assay with 30 μL total sample volumes in 0.5 mL microfuge tubes. Transformed pUC19 plasmid (3 μL, N 95% form I) was added to 15 μL of 5 mM Tris-HCl buffer supplemented with 50 mM NaCl (pH 7.5). Serial dilutions of the Ru(II) compounds were prepared in doubly distilled water (ddH_2O) and added in 7.5 μL aliquots to the appropriate tubes to yield final Ru(II) concentrations ranging from 1 to 100 μM. Then, ddH_2O (4.5 μL) was added to bring the final assay volumes to 30 μL. Control samples with no metal complex received 12 μL of water. Sample tubes were kept at 37 °C in the dark or irradiated. Light treatments employed visible light (14 J cm^{-2}) delivered from a Luzchem LZC-4X photoreactor over the course of 30 min. A softer light dose, relative to that used in the cellular assays, was required to see the topological changes to DNA before the DNA became too distorted to be imaged with the intercalating dye. After treatment, all samples (dark and light) were quenched by the addition of 6 μL of gel loading buffer (0.025% bromophenol blue, 40% glycerol). Samples (11.8 μL) were loaded onto 1% agarose gels cast with 1X TAE (40 mM Tris-acetate, 1 mM EDTA, pH 8.2) and electrophoresed for 30 min at 80 Vcm^{-1} in 1X TAE prior to staining for 30 min in an aqueous solution of 2 μg mL^{-1} EB. The bands were visualized using the Gel Doc-It Imaging system (UVP) with Vision Works software and further processed with the GNU Image Manipulation Program (GIMP).

■ ASSOCIATED CONTENT

Supporting Information

The Supporting Information is available free of charge on the ACS Publications website at DOI: 10.1021/acs.inorgchem.7b00072.

Synthetic procedures; characterization, NMR, and UV/vis data and spectra for all Ru(II) complexes; PDT dose−response curves; phototherapeutic indices for **4a**−**c**, **4h**, **4j**, and **4k** in CCD-1064Sk cells (PDF)

X-ray crystallographic data for **4·PF$_6$** (CIF)

■ AUTHOR INFORMATION

Corresponding Authors

*E-mail: Alison.Thompson@dal.ca. (A.T.)

*E-mail: sherri.mcfarland@acadiau.ca; samcfarl@uncg.edu. (S.A.M.)

ORCID

Alison Thompson: 0000-0003-4231-3446

Notes

The authors declare no competing financial interest.

■ ACKNOWLEDGMENTS

This work was supported by the Natural Sciences and Engineering Research Council of Canada (NSERC).

■ REFERENCES

(1) Storr, T.; Thompson, K. H.; Orvig, C. Design of targeting ligands in medicinal inorganic chemistry. *Chem. Soc. Rev.* **2006**, *35*, 534−544.

(2) Zaki, M.; Arjmand, F.; Tabassum, S. Current and future potential of metallo drugs: Revisiting DNA-binding of metal containing molecules and their diverse mechanism of action. *Inorg. Chim. Acta* **2016**, *444*, 1−22.

(3) Alessio, E. *Bioinorganic Medicinal Chemistry;* Wiley-VCH Verlag GmbH & Co. KGaA, 2011; p 422.

(4) Palermo, G.; Magistrato, A.; Riedel, T.; von Erlach, T.; Davey, C. A.; Dyson, P. J.; Rothlisberger, U. Fighting cancer with transition metal complexes: From naked DNA to protein and chromatin targeting strategies. *ChemMedChem* **2016**, *11*, 1199−1210.

(5) He, L.; Li, Y.; Tan, C.-P.; Ye, R.-R.; Chen, M.-H.; Cao, J.-J.; Ji, L.-N.; Mao, Z.-W. Cyclometalated iridium(iii) complexes as lysosome-targeted photodynamic anticancer and real-time tracking agents. *Chem. Sci.* **2015**, *6*, 5409−5418.

(6) Tan, C.-P.; Lu, Y.-Y.; Ji, L.-N.; Mao, Z.-W. Metallomics insights into the programmed cell death induced by metal-based anticancer compounds. *Metallomics* **2014**, *6*, 978−995.

(7) Wang, C.; Lystrom, L.; Yin, H.; Hetu, M.; Kilina, S.; McFarland, S. A.; Sun, W. Increasing the triplet lifetime and extending the ground-state absorption of biscyclometalated Ir(III) complexes for reverse saturable absorption and photodynamic therapy applications. *Dalton Trans.* **2016**, *45*, 16366−16378.

(8) Trondl, R.; Heffeter, P.; Kowol, C. R.; Jakupec, M. A.; Berger, W.; Keppler, B. K. Nkp-1339, the first ruthenium-based anticancer drug on the edge to clinical application. *Chem. Sci.* **2014**, *5*, 2925−2932.

(9) Howerton, B. S.; Heidary, D. K.; Glazer, E. C. Strained ruthenium complexes are potent light-activated anticancer agents. *J. Am. Chem. Soc.* **2012**, *134*, 8324−8327.

(10) Mari, C.; Pierroz, V.; Ferrari, S.; Gasser, G. Combination of ru(ii) complexes and light: New frontiers in cancer therapy. *Chem. Sci.* **2015**, *6*, 2660−2686.

(11) Glazer, E. C. Light-activated metal complexes that covalently modify DNA. *Isr. J. Chem.* **2013**, *53*, 391−400.

(12) Higgins, S. L. H.; Brewer, K. J. Designing red-light-activated multifunctional agents for the photodynamic therapy. *Angew. Chem., Int. Ed.* **2012**, *51*, 11420−11422.

(13) Knoll, J. D.; Turro, C. Control and utilization of ruthenium and rhodium metal complex excited states for photoactivated cancer therapy. *Coord. Chem. Rev.* **2015**, *282*−*283*, 110−126.

(14) Shi, G.; Monro, S.; Hennigar, R.; Colpitts, J.; Fong, J.; Kasimova, K.; Yin, H.; DeCoste, R.; Spencer, C.; Chamberlain, L.; Mandel, A.; Lilge, L.; McFarland, S. A. Ru(ii) dyads derived from. A-oligothiophenes: A new class of potent and versatile, photosensitizers for pdt. *Coord. Chem. Rev.* **2015**, *282*−*283*, 127−138.

DOI: 10.1021/acs.inorgchem.7b00072
Inorg. Chem. 2017, 56, 4121−4132

(15) Bonnett, R. *Chemical Aspects of Photodynamic Therapy;* Gordon and Breach Science Publishers, 2000.
(16) Hamblin, M. R.; Huang, Y.-Y. *Handbook of Photomedicine;* Taylor & Francis, 2014.
(17) Gollnick, S. O.; Vaughan, L.; Henderson, B. W. Generation of effective antitumor vaccines using photodynamic therapy. *Cancer Res.* **2002**, *62*, 1604−1608.
(18) Gollnick, S. O.; Brackett, C. M. Enhancement of anti-tumor immunity by photodynamic therapy. *Immunol. Res.* **2010**, *46*, 216−226.
(19) Gollnick, S. O. Photodynamic therapy and antitumor immunity. *J. Natl. Compr. Canc. Netw.* **2012**, *10* (Suppl 2), S40−43.
(20) Reginato, E.; Wolf, P.; Hamblin, M. R. Immune response after photodynamic therapy increases anti-cancer and anti-bacterial effects. *World J. Immunol.* **2014**, *4*, 1−11.
(21) Sainuddin, T.; McCain, J.; Pinto, M.; Yin, H.; Gibson, J.; Hetu, M.; McFarland, S. A. Organometallic ru(ii) photosensitizers derived from π-expansive cyclometalating ligands: Surprising theranostic pdt effects. *Inorg. Chem.* **2016**, *55*, 83−95.
(22) Yin, H.; Stephenson, M.; Gibson, J.; Sampson, E.; Shi, G.; Sainuddin, T.; Monro, S.; McFarland, S. A. In vitro multiwavelength pdt with 3il states: Teaching old molecules new tricks. *Inorg. Chem.* **2014**, *53*, 4548−4559.
(23) Reichardt, C.; Pinto, M.; Wächtler, M.; Stephenson, M.; Kupfer, S.; Sainuddin, T.; Guthmuller, J.; McFarland, S. A.; Dietzek, B. Photophysics of ru(ii) dyads derived from pyrenyl-substitued imidazo-[4,5-f][1,10]phenanthroline ligands. *J. Phys. Chem. A* **2015**, *119*, 3986−3994.
(24) Peña, B.; David, A.; Pavani, C.; Baptista, M. S.; Pellois, J.-P.; Turro, C.; Dunbar, K. R. Cytotoxicity studies of cyclometallated ruthenium(II) compounds: New applications for ruthenium dyes. *Organometallics* **2014**, *33*, 1100−1103.
(25) Albani, B. A.; Peña, B.; Dunbar, K. R.; Turro, C. New cyclometallated Ru(II) complex for potential application in photochemotherapy? *Photochem. Photobiol. Sci.* **2014**, *13*, 272−280.
(26) Noffke, A. L.; Habtemariam, A.; Pizarro, A. M.; Sadler, P. Designing organometallic compounds for catalysis and therapy. *Chem. Commun.* **2012**, *48*, 5219−5246.
(27) Huang, H.; Zhang, P.; Chen, H.; Ji, L.; Chao, H. *Chem. - Eur. J.* **2015**, *21*, 715−725.
(28) Dias, A. R.; Veiros, L. F. Are cyclopentadienyl complexes more stable than their pyrrolyl analogues? *J. Organomet. Chem.* **2005**, *690*, 1840−1844.
(29) Kotora, M. Metallocene-catalyzed selective reactions. *Top. Organomet. Chem.* **2004**, *8*, 57−137.
(30) Kowalski, K. Recent developments in the chemistry of azaferrocenes. *Coord. Chem. Rev.* **2010**, *254*, 1895−1917.
(31) Dias, A. R.; Ferreira, A. P.; Veiros, L. F. Bonding and fluxionality in group-4 metal complexes with pyrrolyl ligands. *C. R. Chim.* **2005**, *8*, 1444−1452.
(32) Ferreira da Silva, J. L.; Galvao, A. C.; Ferreira, A. P.; Galvao, A. M.; Dias, A. R.; Gomes, P. T.; Salema, M. S. Effect of ancillary ligands in the hapticity of the pyrrolyl ligand in [Ti(pyrrolyl) (nme2)xcl3-x] (x = 0, 1, 2, 3) complexes. *J. Organomet. Chem.* **2010**, *695*, 1533−1540.
(33) King, R. B.; Bisnette, M. B. Organometallic chemistry of the transition metals. Viii. Π-cyclopentadienyl-π-pyrrolyliron and π-cyclopentadienyl-π-indenyliron. *Inorg. Chem.* **1964**, *3*, 796−800.
(34) Crewdson, P.; Gambarotta, S.; Yap, G. P. A.; Thompson, L. K. Dinuclear and octanuclear mn(ii) complexes with μ2-c, μ2-n-(pyrrolide), and μ-η1:H5-(pyrrolide) bridges: A structural and magnetic study. *Inorg. Chem.* **2003**, *42*, 8579−8584.
(35) Ilango, S.; Vidjayacoumar, B.; Gambarotta, S.; Gorelsky, S. I. Low-valent vanadium complexes of a pyrrolide-based ligand. Electronic structure of a dimeric v(i) complex with a short and weak metal-metal bond. *Inorg. Chem.* **2008**, *47*, 3265−3273.
(36) Lundrigan, T.; Jackson, C. L. M.; Uddin, M. I.; Tucker, L. A.; Ali, A. A.-S.; Linden, A.; Cameron, T. S.; Thompson, A. Synthesis of heteroleptic pyrrolide/bipyridyl complexes of ruthenium(II). *Can. J. Chem.* **2012**, *90*, 693−700.
(37) Mirebeau, J.-H.; Le Bideau, F.; Marrot, J.; Jaouen, G. Synthesis of rhenium carbonyl complexes bearing substituted pyrrolyl ligands. *Organometallics* **2008**, *27*, 2911−2914.
(38) Paine, J. B., III; Dolphin, D. Pyrrole chemistry. An improved synthesis of ethyl pyrrole-2-carboxylate esters from diethyl aminomalonate. *J. Org. Chem.* **1985**, *50*, 5598−604.
(39) Groves, B. R.; Smithen, D. A.; Cameron, T. S.; Thompson, A. Thionation reactions of 2-pyrrole carboxylates. *RSC Adv.* **2016**, *6*, 69691−69697.
(40) Takaya, H.; Kojima, S.; Murahashi, S.-I. Rhodium complex-catalyzed reaction of isonitriles with carbonyl compounds: Catalytic synthesis of pyrroles. *Org. Lett.* **2001**, *3*, 421−424.
(41) Katritzky, A. R.; Sobiak, S.; Marson, C. M. Comparative study of the carbon-13 nuclear magnetic resonance shifts of carbonyl and thiocarbonyl compounds. *Magn. Reson. Chem.* **1988**, *26*, 665−70.
(42) Biner, M.; Buergi, H. B.; Ludi, A.; Roehr, C. Crystal and molecular structures of [Ru(bpy)3](pf6)3 and [ru(bpy)3](pf6)2 at 105 k. *J. Am. Chem. Soc.* **1992**, *114*, 5197−203.
(43) Li, G.; Ray, L.; Glass, E. N.; Kovnir, K.; Khoroshutin, A.; Gorelsky, S. I.; Shatruk, M. Synthesis of panchromatic ru(ii) thienyl-dipyrrin complexes and evaluation of their light-harvesting capacity. *Inorg. Chem.* **2012**, *51*, 1614−1624.
(44) Smalley, S. J.; Waterland, M. R.; Telfer, S. G. Heteroleptic dipyrrin/bipyridine complexes of ruthenium(II). *Inorg. Chem.* **2009**, *48*, 13−15.
(45) Kerscher, T.; Kluefers, P.; Kuegel, W. Hydrogen-bond thio acceptors in o-methyl 3,4-dimethylpyrrole-2-thiocarboxylate. *Acta Crystallogr., Sect. E: Struct. Rep. Online* **2007**, *63* (o4217), o4217.
(46) Juris, A.; Campagna, S.; Balzani, V.; Gremaud, G.; von Zelewsky, A. Absorption spectra, luminescence properties, and electrochemical behavior of tris-heterolepticruthenium(11) polypyridine complexes. *Inorg. Chem.* **1988**, *27*, 3652−3655.
(47) Matsuoka, M. *Infrared Absorbing Dyes;* Springer, 1990.
(48) Bhattacharyya, D.; Chakraborty, S.; Munshi, P.; Lahiri, G. K. Ruthenium(ii/iii) bipyridine complexes incorporating thiol-based imine functions: Synthesis, spectroscopic and redox properties. *Polyhedron* **1999**, *18*, 2951−2959.
(49) Ohno, A.; Koizumi, T.; Ohnishi, Y.; Tsuchihashi, G. Electronic spectra of o-alkyl thiobenzoates and their derivatives. *Bull. Chem. Soc. Jpn.* **1969**, *42*, 3556−8.
(50) Sullivan, B. P.; Salmon, D. J.; Meyer, T. J. Mixed phosphine 2,2′-bipyridine complexes of ruthenium. *Inorg. Chem.* **1978**, *17*, 3334−41.
(51) Yu, H.-J.; Huang, S.-M.; Li, L.-Y.; Jia, H.-N.; Chao, H.; Mao, Z.-W.; Liu, J.-Z.; Ji, L.-N. Synthesis, DNA-binding and photocleavage studies of ruthenium complexes [ru(bpy)2(mitatp)]2+ and [ru(bpy)-2(nitatp)]2+. *J. Inorg. Biochem.* **2009**, *103*, 881−890.
(52) Lincoln, R.; Kohler, L.; Monro, S.; Yin, H.; Stephenson, M.; Zong, R.; Chouai, A.; Dorsey, C.; Hennigar, R.; Thummel, R. P.; McFarland, S. A. Exploitation of long-lived 3il excited states for metal-organic photodynamic therapy: Verification in a metastatic melanoma model. *J. Am. Chem. Soc.* **2013**, *135*, 17161−17175.
(53) Saha, S.; Mallick, D.; Majumdar, R.; Roy, M.; Dighe, R. R.; Jemmis, E. D.; Chakravarty, A. R. Structure-activity relationship of photocytotoxic iron(III) complexes of modified dipyridophenazine ligands. *Inorg. Chem.* **2011**, *50*, 2975−2987.
(54) Croke, D. T.; Perrouault, L.; Sari, M. A.; Battioni, J. P.; Mansuy, D.; Helene, C.; Le Doan, T. Structure-activity relationships for DNA photocleavage by cationic porphyrins. *J. Photochem. Photobiol., B* **1993**, *18*, 41−50.
(55) Praseuth, D.; Gaudemer, A.; Verlhac, J.-B.; Kraljic, I.; Sissoeff, I.; Guille, E. Photocleavage of DNA in the presence of synthetic water-soluble porphyrins. *Photochem. Photobiol.* **1986**, *44*, 717−724.
(56) Sainuddin, T.; Pinto, M.; Yin, H.; Hetu, M.; Colpitts, J.; McFarland, S. A. Strained ruthenium metal−organic dyads as photocisplatin agents with dual action. *J. Inorg. Biochem.* **2016**, *158*, 45−54.
(57) Qiu, K.; Yu, B.; Huang, H.; Zhang, P.; Huang, J.; Zou, S.; Chen, Y.; Ji, L.; Chao, H. A dendritic nano-sized hexanuclear ruthenium(II)

complex as a one- and two-photon luminescent tracking non-viral gene vector. *Sci. Rep.* **2015**, *5*, 10707.

(58) Shi, Y.; Zhou, L.; Wang, R.; Pang, Y.; Xiao, W.; Li, H.; Su, Y.; Wang, X.; Zhu, B.; Zhu, X.; Yan, D.; Gu, H. In situ preparation of magnetic nonviral gene vectors and magnetofection in vitro. *Nanotechnology* **2010**, *21*, 115103.

(59) Silva, G. A.; Oliveira, A. V.; Bitoque, D. B.; Silva, A. P.; Rosa da Costa, A. M. Transfection efficiency of chitosan and thiolated chitosan in retinal pigment epithelium cells: A comparative study. *J. Pharm. BioAllied Sci.* **2013**, *5*, 111−118.

DOI: 10.1021/acs.inorgchem.7b00072
Inorg. Chem. 2017, 56, 4121−4132